Reducing the energy consumption of electric buses with design choices and predictive driving

Klaus Kivekäs, *Student member, IEEE*, Antti Lajunen, *Senior member, IEEE*, Francesco Baldi, *Member, IEEE*, Jari Vepsäläinen, *Student member, IEEE,* Kari Tammi, *Member, IEEE*

***Abstract*—Transportation electrification is increasing and recently more focus has been directed on heavy vehicles and especially on city buses. Battery electric buses are inherently more energy efficient than diesel buses and the efficiency can be further increased by different methods. This paper evaluates the energy consumption reductions that are achievable with an aluminum chassis, low-drag body, low-rolling-resistance class C tires, heat pump, and predictive driving. A simulation model of a generic electric bus was developed in the Simulink software. Simulations were carried out on various types of driving cycles in cold (-10 °C) and warm conditions (20 °C). A novel nonlinear model predictive control problem formulation was created for minimizing the energy consumption of an electric bus. Using a heat pump instead of an electric heater provided the highest energy savings in the cold conditions with an average consumption reduction of 12.7 %. The results indicated that a heat pump is particularly effective on low-speed bus routes. However, the class C tires and aluminum chassis provided higher energy savings than the heat pump in the warm conditions. The low-rolling-resistance tires achieved the most robust energy savings. The aluminum chassis reduced the energy consumption more than the class C tires, but the benefit of the lighter chassis was shown to also correlate strongly with the aggressiveness of the driving. The results showed that a low-drag body is a potential method for consumption reduction on high-speed bus routes. Predictive driving was found to reduce the average consumption by 9.5 % at -10 °C when using 10-second prediction and control horizons.[1]**

***Index Terms*—Aerodynamics, electric vehicles, energy consumption, predictive control, tires, vehicle driving**

I. Introduction

The urgent need for reducing the environmental impact of transportation has made battery electric buses an interesting option to replace traditional diesel buses [1]. In recent years, electric buses have developed at a fast pace together with advanced charging technologies [2], [3]. Increasing amounts of demonstration fleets of electric buses have been deployed worldwide [4], [5]. Furthermore, some cities have already decided to electrify their bus fleets in the coming years, e.g., Paris, Amsterdam, and Shenzhen [6]. One major advantage of transport electrification is the higher energy conversion efficiency of the powertrain, which typically consists of a battery pack, inverter, electric motor (EM), and differential gear. Recent research studies indicate that electric buses can already achieve higher cost effectiveness than diesel buses depending on the operating conditions [7].

Previous publications have shown that the energy consumption of electric vehicles (EVs) can vary significantly due to the operating conditions [8]–[10]. Although electric buses are highly energy efficient, their consumption is also influenced by the driving pattern, passenger load, and particularly by the ambient temperature [11]. As there is much less waste heat produced by the electric powertrain in comparison to a diesel engine, a significant portion of the battery energy has to be sacrificed for heating the cabin when the ambient temperature is particularly low [12], [13]. Alternatively, a fuel heater can heat the cabin. However, the choice is less-than-ideal due to the pollution caused by the heater. Cabin thermal management has been increasingly studied among electric vehicles [14], [15]. Different technological solutions to improve the energy efficiency of the thermal management of the cabin have been proposed [12]. For electric buses, heat pumps have been identified as a key technology to efficiently ensure passenger comfort and increase thermal energy efficiency [16]. However, the downside of heat pumps is that in very cold ambient conditions ($T < -20\,℃$) their efficiency is not usually any better than that of electric heaters [17].

This research evaluates different methods to improve the energy efficiency of battery electric buses. Four key design and component-choice-related methods are identified and compared. Furthermore, the potential energy consumption reductions provided by predictive driving are examined. To that end, a novel nonlinear model predictive control (NMPC) algorithm is presented. The impact of the length of the prediction and control horizons is examined. The results provide novel insights about the most effective ways to reduce the energy consumption of electric buses and how to optimally formulate an NMPC algorithm for an electric bus.

This paper is a continuation of our previous research focusing on the energy consumption of electric buses [18]. In this paper, we begin with a literature review of electric bus energy consumption and driving optimization studies. In section III, a simulation model of a generic electric bus is presented. Then, four key methods are identified for reducing the energy

[1]Manuscript submitted January 18, 2019. This work was supported in part by Business Finland under grant 9977/31/2016, Henry Ford Foundation Finland under grant 20170122, and Yrjö and Senja Koivunen Foundation under grant 27/09/2017.

K. Kivekäs, J. Vepsäläinen, and K. Tammi are with the Department of Mechanical Engineering at Aalto University, Espoo, 02150 FI (e-mail: klaus.kivekas@aalto.fi, jari.vepsalainen@aalto.fi, kari.tammi@aalto.fi). A. Lajunen is with the Faculty of Agriculture and Forestry at University of Helsinki, Helsinki, 00790 FI (e-mail: antti.lajunen@helsinki.fi). F. Baldi is with École polytechnique fédérale de Lausanne, Sion, CH (e-mail: francesco.baldi86@gmail.com).

consumption through design and component choices. In section IV, the novel NMPC algorithm is described. The simulation results are presented and discussed in section V. In the final section, conclusions are drawn and possible future developments considered.

II. State-of-the-Art

In recent years, several studies have been conducted to examine the different factors influencing the energy consumption of EVs. More and more simulation tools are dedicated to electric powertrain modeling and optimization [19]. The significance of ambient temperature to the energy use of EVs has been noted in various papers. Younes et al. [20] analyzed measurement data from an electric car and found that the most influential factors to energy consumption were driving aggressiveness and ambient temperature. Fiori et al. [21] found in a simulation study that the energy consumption of an electric car could increase by 32 % when the ambient temperature decreased from 25 to -5 °C. The increased heating power demand in cold conditions leads to a proportionally higher increase in energy consumption compared to conventional internal combustion engine (ICE) vehicles. Several studies have demonstrated that the influence of ambient temperature is even more severe on electric buses compared to electric cars because of higher heating power requirements [9], [16], [22], [23]. The energy consumption variations caused by the variations in heating, ventilation, and air conditioning (HVAC) system power demand must be carefully considered when assessing the feasibility of deploying electric buses [3]. One approach to mitigate this issue is to use a heat pump instead of conventional HVAC systems, as a heat pump can operate at a significantly higher efficiency in most conditions [16].

Rolling resistance has also been shown to be one of the most significant sources of energy losses in electric cars and buses [24], [25]. Lajunen and Tammi [25] conducted a simulation analysis of electric buses that showed rolling resistance to account for approximately 25-30 % of the energy losses depending on the driving cycle. Aerodynamic drag could represent between 3 to 25 % of the total losses. The aerodynamic losses are highly dependent on the average speed of the driving cycle.

Vepsäläinen [26] investigated the differences in driving styles between diesel bus and electric bus operation. He found that electric buses are generally driven more aggressively, as the instantaneous peak torque and fast response invite higher accelerations. On the other hand, several studies have indicated that the energy consumption of electric buses is influenced less by the driving cycle compared to diesel buses in urban and suburban operation [27]–[30]. The lower sensitivity to driving cycle uncertainty is largely explained by the ability to perform regenerative braking. However, the stop frequency is still one of the most significant factors in the energy consumption of electric buses [31], [32]. It has also been demonstrated that the energy consumption influence of the aggressiveness of the driving is magnified by increases in the passenger load [25].

Earlier efforts to reduce the energy consumption of city buses via driving improvements involved incentive-based systems for bus drivers. Liimatainen [33] proposed a peer-competition-based system but noted the significant ethical concerns caused by potentially making the workplace more competitive. Additionally, it is challenging to set fair targets for energy consumption due to the uncertainty involved in bus operation [34]. Thus, automated driving optimization is now seen as a better alternative for reducing city bus energy consumption.

Various papers have presented methods for driving optimization using dynamic programming (DP) although they have mostly focused on passenger cars [35]–[37]. Lajunen [38] developed a distance-based DP algorithm to optimize the Braunschweig driving cycle for an electric bus and found that the energy usage could be reduced by 19 %. However, DP is typically computationally-intensive, and it requires full knowledge of the entire driving route [39]. Consequently, DP is not suited for real-time optimization. Ozatay et al. [40] proposed using cloud computing to enable enough computing power for real-time online use of DP. Doan et al. [41] developed an iterative DP algorithm for optimizing the driving of EVs, which they demonstrated to be fast enough for real-time use.

Model predictive control (MPC) has been widely used in vehicular applications. For example, it has been utilized to optimize the energy management of series, parallel, and power split hybrid vehicles [42]–[46]. Additionally, MPC has been employed for yaw control, vehicle following, path planning and tracking for collision avoidance, intervehicular traffic flow management, thermal management, as well as charging optimization of EVs [47]–[55]. Furthermore, MPC has been used in driving optimization applications. Kamal et al. [56] developed a time-based nonlinear model predictive control (NMPC) algorithm to optimize the driving of a conventional ICE passenger car in traffic. Fuel consumption was approximated as a function of speed and positive acceleration using a third-degree polynomial. NMPC has also been proposed for use in an ecological adaptive cruise controller for plug-in power split hybrid vehicles in congested conditions [57]. In the developed algorithm, fuel consumption was estimated as a function of engine power and vehicle speed with a second-degree polynomial, and the EM efficiencies were assumed constant. Held et al. [58] developed a linear-MPC-based driving optimization algorithm for heavy EVs. With a horizon length of 500 m, the distance-based MPC was shown to achieve energy savings similar to offline optimization using Pontryagin's minimum principle (PMP). Zhang et al. [59] proposed an explicit MPC method for controlling EVs. Additionally, they employed a Bayes network model to predict the movement of the preceding vehicle. The results demonstrated that the energy savings can be significantly improved with a better understanding of the approaching traffic environment. Lim et al. [39] proposed the use of a two-stage optimization algorithm based on quadratic programming (QP). First, the driving profile of the entire route would be optimized before departure. Traffic would then be accounted for in local adaptation with a short optimization horizon.

While the different factors affecting the energy consumption of electric buses have been examined in previous papers, a direct comparison between the energy savings achieved with

the various methods has not been conducted. This paper aims to fill that research gap by comparing the energy savings achieved with a lightweight chassis, low-rolling-resistance tires, low-drag body, heat pump, and NMPC driving optimization. A novel formulation for the NMPC control problem is presented using the nonlinear MPC controller in MATLAB/Simulink, which was launched with the R2018b version of the software [60].

III. Electric Bus Simulation Model

A simulation model of a standard 12-meter long battery electric bus was developed in the Simulink software. The simulation model is based on equations (1)–(12). The model takes as its inputs the EM torque demand, mechanical braking force, and road grade, and it outputs the speed of the vehicle as well as the battery power.

In the model, the acceleration of the vehicle (a) is calculated as follows:

$$a(t) = \frac{F_w(t) - F_R(t)}{m + J_{tot}/r_d^2} \tag{1}$$

where t is time, m is the total mass of the bus, F_W is the tractive force at the driven wheels, F_R is the sum of the resistive forces, J_{tot} is the total moment of inertia superimposed at the driven axle, and r_d is the dynamic radius of the wheels. The total mass is the sum of the curb weight (m_{curb}) of the vehicle and the passenger load (m_{pass}):

$$m = m_{curb} + m_{pass}. \tag{2}$$

The resistive forces are calculated as:

$$F_R(t) = mg(f_{rr}\cos\alpha(t) + \sin\alpha(t)) + \rho c_D A v(t)^2/2 \tag{3}$$

where g is the gravitational acceleration (9.81 m/s^2), f_{rr} is the rolling resistance coefficient, α is the road grade, ρ is the density of air, c_D is the drag coefficient, A is the frontal area, and v is the speed of the bus. The rolling resistance term is zero if speed is zero. The tractive force is defined as:

$$F_w(t) = T_M(t) i_g i_{fd} H_{dt}\big(P_M(t)\big)/r_d + F_B(t) \tag{4}$$

where T_M is the EM torque, i_g is the gear ratio of the gearbox, i_{fd} is the gear ratio of the final drive, and F_B is the mechanical brake force. The variable H_{dt}, which represents the efficiency of the drivetrain, depends on the EM output power P_M in the following way:

$$\begin{cases} H_{dt} = \eta_g \eta_{fd}, & P_M(t) \geq 0 \\ H_{dt} = 1/(\eta_g \eta_{fd}), & P_M(t) < 0 \end{cases} \tag{5}$$

where η_g and η_{fd} are the efficiencies of the gearbox and final drive. The rotational speed of the motor is calculated as:

$$\omega_M(t) = v(t) i_g i_{fd}/r_d. \tag{6}$$

The total power consumption of the battery P_b is calculated as a sum of the battery output power P_{b_o} and the internal losses of the battery P_{b_l}, as shown in (7):

$$P_b(t) = P_{b\_o}(t) + P_{b\_l}(t) = I_b(t)U_b(t) + r_b(t)\big(q_b(t)\big)I_b(t)^2 \tag{7}$$

where I_b is the battery current, U_b is the pole voltage of the battery, and r_b is the internal resistance of the battery as a function of the battery state-of-charge (SOC) q_b. The output power of the battery can also be calculated as:

$$P_{b\_o}(t) = H_M\big(\omega_M(t), T_M(t)\big)T_M(t)\omega_M(t) + P_{aux,total} \tag{8}$$

where $P_{aux,total}$ is the total auxiliary device power demand. The total auxiliary power demand consists of the HVAC power demand (P_{HVAC}) and the power demand of other auxiliary devices ($P_{aux,other}$):

$$P_{aux,total} = P_{HVAC} + P_{aux,other}. \tag{9}$$

The other auxiliary devices include power steering, air compressor, powertrain thermal management, and other electronics. The variable H_M in equation (8) represents the combined efficiency of the EM and the inverter and is defined as:

$$\begin{cases} H_M = \eta_M\big(\omega_M(t), T_M(t)\big), & P_M(t) < 0 \\ H_M = 1/\eta_M\big(\omega_M(t), T_M(t)\big), & P_M(t) \geq 0 \end{cases} \tag{10}$$

where η_M is the efficiency value obtained from the efficiency map. The efficiency map that was used in reference [18] was also used in this simulation model. The battery was modeled with a resistance model. Thus, the model calculates the battery current as:

$$I_b(t) = \frac{U_{voc}\big(q_b(t)\big) - \sqrt{U_{voc}\big(q_b(t)\big)^2 - 4r_b\big(q_b(t)\big)P_{b\_o}(t)}}{2r_b\big(q_b(t)\big)} \tag{11}$$

where U_{voc} is the open-circuit voltage of the battery as a function of the SOC. The SOC is calculated based on the battery current and capacity C_b (in Ah) as:

$$\frac{dq_b}{dt} = I_b(t)/(3600C_b). \tag{12}$$

The model was parameterized based on our previous research [25]. The key technical specifications of the bus model are presented in Table 1. The limits for regenerative braking were defined in the same way as in the model in our previous work

[30]. Full regeneration would be allowed at speeds above 10.8 km/h. Below that speed, the regeneration limit declines linearly until no regeneration is allowed below 5.4 km/h. Similarly, full regeneration is only allowed at decelerations up to 2.5 m/s^2, and partial regeneration is enabled up to 4.0 m/s^2. A motor controller unit enforces these limits as well as the EM power and torque limits. Any excess negative power requested from the motor by the driving controller is converted to mechanical braking force. The power demand $P_{aux,other}$ was defined as 5 kW based on our previous research where the auxiliary device power demand of an electric bus operating in Espoo, Finland was measured [32].

In order to evaluate different design and component-choice-related methods to reduce the energy consumption of electric buses, simulations were carried out with reference parameters and with changes to four key parameters. These parameters were the curb weight, aerodynamic drag, rolling resistance and HVAC power. Table 2 presents the reference and reduced values of these parameters. The reference curb weight was chosen to represent a typical steel chassis bus, and the reduced value would represent an aluminum chassis bus. The weight difference was approximated based on previous works and publicly available bus data [61]–[63]. The reference aerodynamic drag value was chosen to represent a typical city bus with a height of 3.3 m and width of 2.55 m and ride height assumed as 30 cm [63]. The reference drag coefficient was set to 0.8. The value presented in Table II is the frontal area multiplied with the drag coefficient. A low-drag bus was represented with the reduced drag value. A lower body profile can have a frontal area of close to 6 m^2, and it is also known that the drag coefficient tends to reduce with the frontal area [62], [64]. The reference and reduced rolling resistance coefficient values were chosen such that the reference value would represent a typical class E bus tire, and the low-resistance version would represent a more premium class C bus tire. The rolling-resistance-based tire classes are presented in reference [65]. The simulations were run at -10 and 20 °C ambient temperatures. The HVAC power demand values were approximated based on reference [25] where the power demand was approximated as a function of the ambient temperature based on recent literature. The reference HVAC power demand represents an electric heater, and the reduced value represents a heat pump. The HVAC power demand reduction achieved with a heat pump was approximated to be 50 % based on previous works [16], [17]. The HVAC power demand was defined as being constant to approximate the average HVAC power use. In equations (1)–(12), the parameters corresponding to the curb weight, aerodynamic drag, rolling resistance, and HVAC power that were changed in the tests to simulate the effect of the design and component changes are m_{curb}, $c_D A$, f_{rr}, and P_{HVAC}. The drag coefficient c_D and frontal area A were both changed, and the value shown in Table II is the product of the frontal area and the drag coefficient.

Simulations were carried out on 15 different driving cycles. Descriptions of the cycles along with their parameters can be found in reference [18]. A proportional controller was used for controlling the vehicle. The input of the controller was set as the difference between the target speed, which was acquired from the profile of the driving cycle, and the current speed of the bus. The output of the P controller was the EM torque demand. The initial SOC level was set to 80 %.

TABLE I.
TECHNICAL SPECIFICATIONS OF THE ELECTRIC BUS

Description	Value
Battery chemistry and capacity	Titanate Oxide, 60Ah
Battery system specific energy (Wh/kg)	60
Battery energy capacity (kWh)	77.3
Battery system weight (kg)	1295
Motor nominal power (kW)	170
Motor max peak torque (Nm)	1710
Constant aux. power without HVAC (kW)	5.0
Gear reduction	1.75
Final drive ratio	4.72
Tires	275/70/22.5
Tire dynamic radius	0.478
Bus curb weight (kg)	12350
Passenger load (kg)	415

TABLE II.
SIMULATION PARAMETERS

Description	Reference value	Reduced value
Bus curb weight (kg)	12350	10500
Aerodynamic drag (m^2)	6.12	4.30
Rolling resistance coeff.	0.008	0.006
HVAC power at -10 °C (kW)	7.0	3.5
HVAC power at 20 °C (kW)	2.0	1.0

The electric bus model was verified by comparing the energy consumption on the 15 cycles to the energy consumption acquired with the electric bus simulation model used in our previous work [30]. The electric powertrain model utilized in the earlier study had been validated with measurement data acquired from an electric bus operating in Helsinki, Finland. For the comparison, the total auxiliary device power consumption was set to 7 kW and the curb weight to 12350 kg for both models. The comparison between the two models showed that the energy consumption of the model presented in this paper differed on average by only 3.5 % from the consumption of the validated model on the 15 cycles. Hence, it can be stated that the energy consumption produced by the simulation model representing a generic electric bus used in this research is in a realistic range. Furthermore, similar modelling approaches for electric vehicles have been used in a variety of previous works, such as in references [7], [21], [59], and [66].

IV. PREDICTIVE DRIVING

As was discussed in section II, energy consumption can be decreased by optimizing the driving mission, thus minimizing the energy consumption on a given operating route [38]. In the case of electric buses, the driving optimization typically focuses on predicting stopping and minimizing powertrain losses. MPC presents two major improvements when compared to standard PID controllers: 1. It allows for the minimization of not only the control error (i.e. difference between actual state and reference state), but also for the control action and, in principle, for any

other variable that the user can be interested in minimizing. 2. It allows including the presence of constraints in the control formulation, hence ensuring that the system stays within its operational boundaries for the whole control horizon.

The classical MPC problem formulation was devised for a quadratic objective, convex equality constraints, linear inequality constraints, and a linear system model [67]. However, there has been increasing focus in recent years on NMPC. In this research, the NMPC controller in Simulink was used for approximating the potential energy savings that are achievable with automated predictive driving. The effect of the length of the prediction and control horizons on the energy consumption was investigated. The Simulink controller uses the sequential quadratic programming (SQP) algorithm to solve the control problem. The problem formulation must be continuous and continuously differentiable. In the controller, the state-space model of the electric bus is defined as:

$$x(k+1) = \begin{cases} x_1(k) + x_2(k)T_s + a(k)T_s^2/2 \\ x_2(k) + a(k)T_s \end{cases} \tag{13}$$

where the first state x_1 is the distance travelled by the bus, the second state x_2 is the speed of the bus, and T_s is the sample time of the controller. The sample time was set to 1 s in this research. The model outputs are defined as being the same as the states. The acceleration at discrete time instant k is defined as:

$$a(k) = \frac{F_w(k) - F_R(k)}{m + J_{tot}/r_d^2}. \tag{14}$$

The resistive forces in (3) are smoothened by approximation:

$$F_R(k) = mg(f_{rr}\cos\alpha(k)\tanh(c_1 x_2(k)) + \sin\alpha(k)) + \rho c_D A x_2(k)^2/2 \tag{15}$$

where the hyperbolic tangent factor in the rolling resistance term drives the term to zero when the speed is zero whilst still keeping the model continuous and continuously differentiable. The multiplier c_1 was set to 5 by testing how high the value could be set without adversely affecting the computation time. An estimate of the road grade at each prediction step must be provided to the controller. The grade is approximated by assuming that the speed stays constant for the duration of the prediction horizon, thus making it possible to acquire the grade for each prediction step from the known road grade versus distance profile. The tractive force is calculated similar to (4) as:

$$F_w(k) = u_1(k) i_g i_{fd} H_{dt,2}\big(u_1(k)\big)/r_d + u_2(k) \tag{16}$$

where the first control variable u_1 is the EM torque output, and the second control variable u_2 is the mechanical brake force. The variable $H_{dt,2}$, which represents the drivetrain efficiency, is defined as:

$$H_{dt,2} = \frac{-\tanh u_1(k) + 1}{2\eta_g\eta_{fd}} + \frac{(\tanh u_1(k) + 1)\eta_g\eta_{fd}}{2}, \tag{17}$$

which approximates (5). The use of hyperbolic tangent to smoothen the equation ensures that the model is continuous and continuously differentiable.

The inequality constraints are defined as:

$$\begin{cases} x_2 \le v_{max,i} + c_{e1}e_s \\ x_2 \ge 0 \\ u_1 \le T_{M,max} \\ u_1 \ge T_{M,min} \\ u_2 \le 0 \\ u_2 \ge F_{B,max} \\ u_1 x_2 i_g i_{fd}/r_d \le P_{M,max} \\ u_1 x_2 i_g i_{fd}/r_d \ge P_{M,min} \\ x_1(k_c + p) \le d_{target} + c_{e2}e_s \\ x_1(k_c + p) \ge d_{target} - c_{e2}e_s \end{cases} \tag{18}$$

where $v_{max,i}$ is the maximum speed on driving segment i, $T_{M,max}$ and $T_{M,min}$ are the maximum and minimum EM torque values, $F_{B,max}$ is the maximum (negative) mechanical brake force, $P_{M,max}$ and $P_{M,min}$ are the maximum and minimum EM power, d_{target} is the target distance, e_s is a slack variable for constraint softening, c_{e1} and c_{e2} are slack coefficients, and k_c is the current instant. For the NMPC simulations, the 15 driving cycles described in section III were used. The cycles were divided into segments between full stops. A full stop was considered to be any stop maneuver where the vehicle is stationary for two seconds or more. A maximum speed limit was defined for each segment as the highest speed on that segment plus 5 km/h. The driving cycles were used to define the target distance for the NMPC controller. The target was set as the distance travelled on the original cycle at the time instant of the end of the prediction horizon. Stops were handled such that the target distance would not be allowed to increase until one second before the beginning of the next acceleration in the original cycle. By defining the target distance in this way, the distance of each segment would be practically identical to the distance of the segment in the original cycle.

The cost function in the NMPC controller is defined as:

$$\begin{aligned} f = \sum_{k=1}^{p} \Big(& c_{f1} H_{m'} u_1(k)\big(\omega_M(k) + \omega_M(k+1)\big)/2 \\ & + \big(c_{f2}u_2(k)\big)^2 + \big(c_{f3}x_2(k+1)\big)^2 \\ & + c_{f4}e_s^2 + \big(c_{f5}\big(u_1(k) - u_1(k-1)\big)\big)^2 \\ & + \big(c_{f6}\big(u_2(k) - u_2(k-1)\big)\big)^2 \Big) \end{aligned} \tag{19}$$

where the variable $H_{m'}$ represents the efficiency of the motor and inverter, c_{fi} is the coefficient of the i-th term, and p is the length (in number of time steps) of the prediction horizon. The purpose of the first term is to minimize the energy consumption

by minimizing the input power of the EM. The second term penalizes mechanical brake usage. The aim of the third term is to help with the energy reduction minimization by reducing the aggressiveness of the driving, which can be defined as [30]:

$$A = \sum_{i=1}^{n} \int_{t_{i,1}}^{t_{i,2}} \big(a(t) \cdot v(t)\big)\, dt \Big/ s \tag{20}$$

where n is the number of positive acceleration periods, $t_{i,1}$ and $t_{i,2}$ are the start and end of the i-th positive acceleration period, and s is the total distance of the driving cycle. The driving aggressiveness has been shown to correlate strongly with the energy consumption of city buses in a previous publication [30]. The fourth term in (19) gives a penalty for not respecting the constraints, as the value of the slack variable increases the more the constraints are violated. The purpose of the fifth and sixth terms is to prevent rapidly oscillating control inputs and in so doing maintain a comfortable experience for the passengers. The EM speed ω_M is calculated according to (6). The efficiency-related variable $H_{m'}$ is calculated as:

$$H_{m'} = \frac{\tanh\big(u_1(k)\big) + 1}{2\eta_{m'}(k)} - \frac{\tanh\big(u_1(k)\big) - 1}{2}\eta_{m'}(k) \tag{21}$$

where $\eta_{m'}$ is the approximated value for the combined efficiency of the EM and inverter. The efficiency was approximated as 86.6 %, as that was the average efficiency in the operating region. Equation (21) is a smoothened approximation of (10). It was found that the use of this type of hyperbolic tangent approximation yielded 30 % reduced computation times compared to raising $\eta_{m'}$ to the power of the sign of the EM torque. As the speed of the bus is assumed to never fall below zero, it is sufficient to examine torque rather than power, as their signs are the same.

The values of the coefficients c_{fi} in (19) were determined by manually finding reasonable ranges for the values and then conducting a sweep. For the parameter sweep, the H58E cycle was used because it is the most average of the cycles in terms of aggressiveness, average speed, and stop frequency. Prediction and control horizons of 2, 4, 6, 8, and 10 s were tested in order to examine the influence of the horizon length on the energy consumption and computation time. Horizons longer than 10 s were not considered due to computational inefficiency. Default parameters provided by MATLAB were used for the SQP solver, including a maximum limit of 400 iterations. The ambient temperature was set to -10 °C for the NMPC predictive driving simulations.

The simulation tests were conducted in the following way. First, the design and component-choice related methods discussed in section III were tested. The results of the tests are presented in section V.A. Then, the predictive driving tests were conducted, and the acquired results are shown in section V.B. Finally, the predictive driving and the four design and component-related methods were used simultaneously to observe the magnitude of the consumption reductions that are achievable when utilizing all of the possible methods together. The results are presented in section V.C.

V. Results and Discussion

A. Design and component simulations

The simulation results were analyzed in order to evaluate the influence of the selected key factors on energy consumption. The distribution of energy losses on the 15 driving cycles in cold and warm conditions using the reference parameter values is presented in Fig. 1 in the order of increasing total energy consumption. The road grade was defined for the cycles marked with a star in the x-axis label. The losses were calculated by using the following six main categories: battery, auxiliary devices, powertrain (including EM, inverter, and gear reductions), rolling resistance, mechanical braking, and aerodynamic resistance. These results clearly show that the auxiliaries, powertrain, and rolling resistance caused the majority of the losses on all of the cycles. The powertrain losses varied between 17.5 and 24.4 % of the total losses at -10 °C and between 22.3 and 29.4 % at 20 °C. Auxiliary device power demand accounted for between 24.2 and 57.6 % of the losses on the cycles in the cold conditions. At 20 °C, the auxiliary losses caused 16.3–44.5 % of the losses. The highest auxiliary consumption, which was 1.1 kWh/km at -10 °C and 0.64 kWh/km at 20 °C, occurred on the Manhattan (MAN) cycle. Rolling resistance accounted for between 14.6 and 24.6 % of the losses in the cold conditions and between 19.3 and 30.7 % in the warm conditions. The rolling resistance losses varied

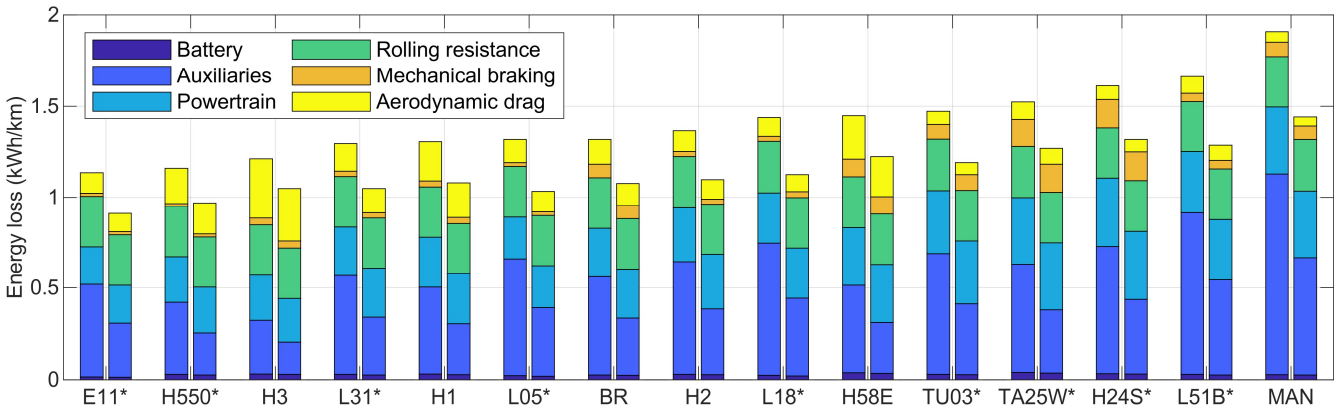

Fig. 1. Distribution of energy losses on the 15 driving cycles with reference parameter values and proportional controller at -10 °C (left) and 20 °C (right).

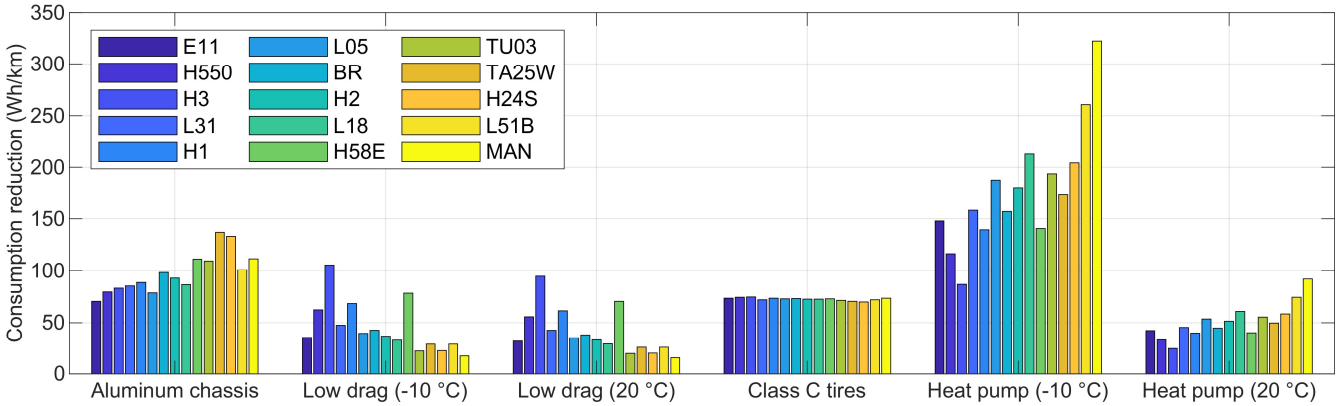

Fig. 2. Influence of the key parameters on energy consumption decrease in all simulated cycles using the proportional controller.

between 278.0 and 278.3 Wh/km. Rolling resistance losses are highly consistent because they are caused by a constant force, and the only variation is caused by road elevation, as can be deduced from equation (3). On the other hand, the aerodynamic drag losses varied significantly. The lowest drag losses occurred on the MAN cycle where they were only 2.9 % of the total losses at -10 °C and 3.5 % at 20 °C. The drag losses were highest on the Helsinki 3 (H3) cycle at 323 and 290 Wh/km at -10 and 20 °C. These values equaled to 26.7 and 27.7 % of the total losses. As the results demonstrate, the higher the average speed of the cycle, the higher the drag losses and the lower the auxiliary losses are. The higher air density in colder conditions also has a minor impact on the drag losses. Mechanical braking caused between 1.4 and 10.0 % of the total losses on the cycles at -10 °C and between 1.7 and 12.2 % at 20 °C. Certain cycles, such as Tampere 25 (TA25W) and Helsinki 24 (H24) feature a significant number of aggressive braking maneuvers that require deploying the mechanical brakes. On all the cycles, battery losses were minimal and only accounted for 1.3 to 2.6 % of the losses in the cold conditions and 1.5–2.9 % in the warm conditions. The overall energy consumption ranged from 1.13 to 1.91 kWh/km with an average of 1.41 kWh/km at -10 °C. In the warm conditions, the range was 0.91–1.44 kWh/km, and the average was 1.14 kWh/km.

Each of the four design and component-related changes shown in Table II were simulated on the 15 driving cycles, and the energy consumption results are presented in Fig. 2. The average consumption reductions provided by the aluminum chassis, low-drag body, class C tires, and heat pump were 98, 45, 73, and 179 Wh/km in the cold conditions. In the warm conditions, the low-drag body reduced the consumption by 40 Wh/km and the heat pump by 51 Wh/km on average. There was virtually no change in the energy savings achieved by the aluminum chassis and low-rolling-resistance tires between the cold and warm conditions. While the heat pump did provide the highest reductions at -10 °C, it lost out to the aluminum chassis and class C tires at 20 °C. Based on previous publications, it is known that HVAC power requirements are low in particular between temperatures 5 and 20 °C [25]. The results also show that the consumption reductions provided by the heat pump were strongly dependent on the driving cycle. The lowest energy use reduction occurred on the H3 cycle with an improvement of 87 Wh/km in the cold conditions and 25 Wh/km in the warm conditions. The highest improvement was seen on the low-speed MAN cycle at 322 Wh/km at -10 °C and 92 Wh/km at 20 °C.

On the other hand, the results demonstrate that the energy use reductions provided by class C tires are highly robust. As can be seen in Fig. 2, the driving cycle had barely any influence on the amount of energy use reduction provided by the tire choice. The effect of the aluminum chassis on the energy consumption was also reasonably consistent with the values ranging between 71 and 137 Wh/km. However, it is worth noting that the consumption reduction contribution correlated strongly with the aggressiveness of the driving cycle with the Pearson correlation coefficient being 0.94. The low-drag body brought the lowest average energy use reductions in both conditions. The consumption reduction correlated strongly with the average driving speed of the cycle with the Pearson coefficient being 0.95. The energy use reductions achieved with the low-drag body ranged from 17 to 106 Wh/km at -10 °C and from 16 to 95 Wh/km at 20 °C.

The results demonstrate that the heat pump can achieve the highest energy savings, but it is at its most effective on low-speed routes and in cold conditions. The aluminum chassis provides a relatively robust energy efficiency improvement, and it reduces the influence of the driving style on the energy consumption, as evidenced by the high correlation with the driving aggressiveness. The low-drag body achieves significant consumption reductions only in high-speed driving, so it is not particularly beneficial on urban bus routes. Low-rolling-resistance tires provide the most robust energy efficiency improvements and are thus recommended to be used regardless of the route type.

B. Predictive driving

The 15 driving cycles were simulated at -10 °C using 2, 4, 6, 8, and 10-second prediction and control horizons for the NMPC controller. An example of an MPC-optimized cycle is shown in Fig. 3, which features the Espoo 11 (E11) cycle. The distributions of the energy consumption reductions and computational speeds achieved using the different horizon lengths are presented in Fig. 4. The average energy consumption reductions achieved were 20, 68, 97, 120, and 138

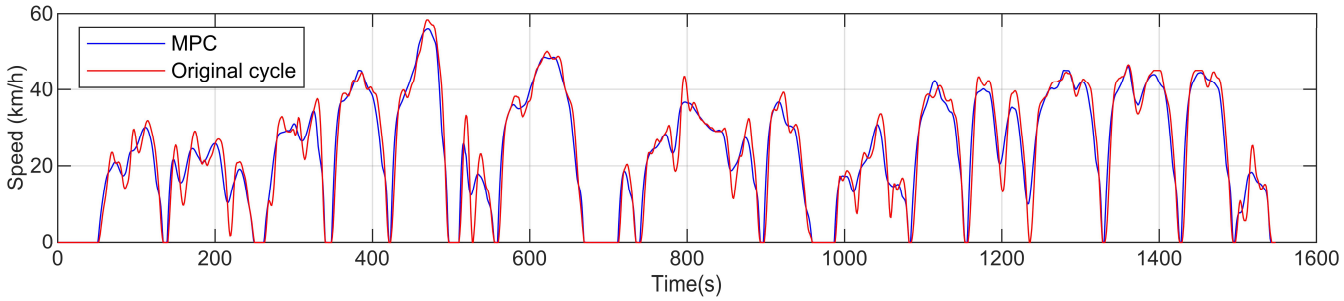

Fig. 3. NMPC optimization on the E11 cycle with 10-second prediction and control horizons.

Wh/km with the 2, 4, 6, 8, and 10-second horizons. It was found that the relationship between the average simulation speed and the consumption reduction with the different horizon lengths was directly proportional, with a linear model fit having an R^2 value of 0.9963. The result demonstrates that it is desirable to have as long a horizon as possible in order to maximize the energy efficiency.

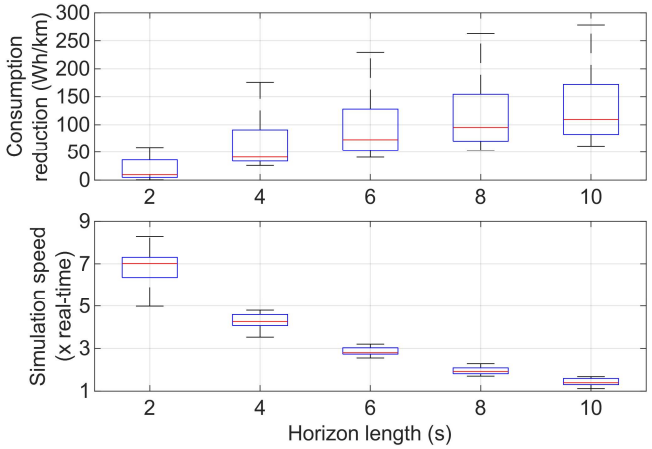

Fig. 4. Distributions of the average consumption reductions and simulation speeds achieved with different horizon lengths on the 15 driving cycles.

When using the simple proportional controller instead of the NMPC controller, the simulation model was capable of performing approximately 350 times faster than real-time. Hence, it can be deduced that the controller caused the vast majority of the computational effort required in the NMPC simulations. The simulations were run with an Intel Xeon E3-1231 v3 @ 3.4 GHz processor.

The loss distributions were further examined in the case of the 10-second horizon. The majority of the energy consumption reductions came from reduced powertrain losses. The average powertrain loss reduction was 74 Wh/km or 24 %. Mechanical braking losses were reduced between 16 and 77 % depending on the cycle. In the original cycles, the highest amount of mechanical braking losses was 10.4 times as high as on the cycle with the lowest mechanical braking losses. With the NMPC, that factor was cut down to less than half (5.0). Aerodynamic drag losses were reduced by 4–28 % and battery losses by 23–52 % on the 15 cycles. The overall average energy consumption reduction achieved with predictive driving was 9.5 %. The percentage varied between 5.4 % and 17.4 % on the 15 cycles with the highest savings occurring on the H24S cycle and the lowest on the E11 cycle. Overall, the results demonstrate that predictive driving can provide worthwhile energy efficiency improvements, as the average consumption reduction with a 10-second horizon was higher than with the design and component-related methods with the exception of the heat pump.

C. Combining predictive driving and the design and component-choice methods

Finally, the cycles were simulated using both the design and component-related methods and NMPC simultaneously in order to examine the total energy use reductions that could be achieved with all possible methods being utilized. A horizon length of 10 seconds was used in the NMPC controller in these tests. The distribution of losses on the cycles is presented in Fig. 5. The overall average energy use reduction was 492 Wh/km or

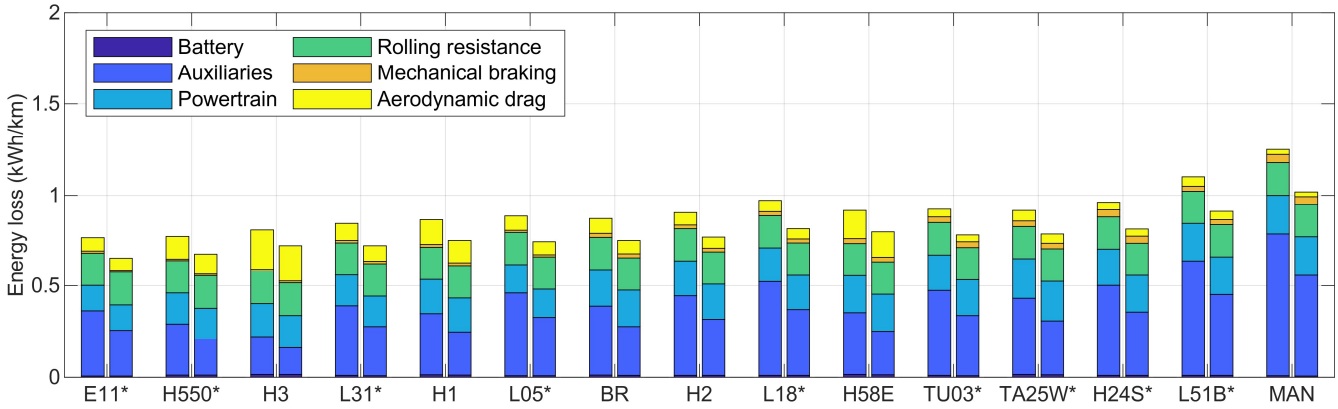

Fig. 5. Distribution of energy losses on the 15 cycles using the design and component-related methods as well as NMPC at -10 °C (left) and 20 °C (right).

34.9 % at -10 °C and 358 Wh/km or 31.4 % at 20 °C. The percentage varied between 32.3 and 40.3 % in the cold conditions and between 27.4 and 38.1 % in the warm conditions. These results indicate that there is significant room for improvement in electric bus energy efficiency with the right design and component choices as well as driving optimization.

Certain limitations in this study limited the scope of the results. Firstly, while the 15 driving cycles feature various types of driving, a higher number of cycles would give a more complete picture of the effects of the different energy efficiency improvement methods. Furthermore, the target distance for the NMPC was obtained from the existing driving cycles, but in order to implement the NMPC in a real application, a method for determining the target distance dynamically would have to be developed along with incorporating safe vehicle-following. However, the NMPC implementation in this paper was considered to provide a good approximation of real NMPC use, as the driving was constrained by the characteristics of the original cycle.

VI. Conclusions

The energy consumption of a standard 12-meter long electric bus was evaluated based on simulations in different types of driving cycles using MATLAB and Simulink. The influence of four key design and component choices were investigated in detail: aluminum chassis, low-drag body, class C tires, and heat pump. The average consumption reductions achieved with the four methods at -10 °C were 7.0, 3.2, 5.2, and 12.7 %. At 20 °C, the reductions were 8.6, 3.5, 6.4, and 4.5 %.

The simulation results clearly indicated that the auxiliary power has a significant influence on energy consumption. Furthermore, the influence is heavily dependent on the driving cycle and the ambient temperature. On low-speed driving cycles in cold conditions, the heat pump achieved significantly higher energy use reductions than the other methods. It can thus be concluded that a heat pump is particularly advantageous on congested urban routes at low ambient temperatures.

The consumption reductions achieved with the low-drag body were also highly dependent on the driving cycle, as the benefit of the reduced aerodynamic drag is speed-dependent. On high-speed cycles, the low-drag body was able to reduce the energy consumption by a similar amount as the low-rolling-resistance tires and the aluminum chassis.

On the other hand, the class C tires were shown to be the most robust way of reducing the consumption. The driving cycle dependence of the benefit of the class C tires was demonstrated to be minimal. The aluminum chassis achieved higher energy use reductions than the low-rolling-resistance tires. However, there was also higher variation in the consumption reductions. The lighter chassis was found to be particularly advantageous in aggressive driving cycles. Hence, it can be concluded that an aluminum chassis makes the energy consumption more robust to variations in the driving aggressiveness.

A novel NMPC problem formulation was presented for minimizing the energy consumption of an electric city bus. A novel method for exploiting hyperbolic tangent in order to ensure continuous model and problem formulations in the NMPC was shown. The energy consumption reductions achievable with predictive driving were examined with simulations using the devised NMPC algorithm. Ten-second prediction and control horizons were shown to achieve an average consumption reduction of 9.5 % at -10 °C. The relationship between the computational speed of the NMPC algorithm and the energy use reductions was found to be directly proportional.

Finally, all of the methods, including the NMPC predictive driving and the design and component-choice related methods, were used simultaneously in order to observe how much the energy consumption of electric buses could be reduced in total. It was found that the consumption could be reduced by 32 to 40 % at -10 °C and by 27 to 38 % at 20 °C. Overall, the results clearly indicate that there is substantial room for improvement in the energy efficiency of electric city buses. Furthermore, consideration must be given for the type of route the bus will be operated on when designing an electric bus so that the most effective consumption reduction methods can be employed.

Future work is required to better understand the lifecycle costs of the proposed energy efficiency improvement methods. Additional methods could also be considered. Further research is needed on the NMPC controller in order to make it viable in real use. A method for dynamically calculating the target distance needs to be devised. Safe vehicle-following should also be implemented. The controller could then be tested in a real application. The sensitivity of the effectiveness of the controller to uncertainty factors could be investigated as well.

References

[1] A. Lajunen and T. Lipman, "Lifecycle cost assessment and carbon dioxide emissions of diesel, natural gas, hybrid electric, fuel cell hybrid and electric transit buses," *Energy*, vol. 106, pp. 329–342, 2016.

[2] M. Mahmoud, R. Garnett, M. Ferguson, and P. Kanaroglou, "Electric buses: A review of alternative powertrains," *Renew. Sustain. Energy Rev.*, vol. 62, pp. 673–684, 2016.

[3] R. Prohaska, K. Kelly, and L. Eudy, "Fast charge battery electric transit bus in-use fleet evaluation," in *2016 IEEE Transportation Electrification Conference and Expo, ITEC 2016*, 2016, pp. 1–6.

[4] J. Miles and S. Potter, "Developing a viable electric bus service: The Milton Keynes demonstration project," *Res. Transp. Econ.*, vol. 48, pp. 357–363, 2014.

[5] U. Guida and S. Leonard, "ZeEUS: Zero Emission Urban Bus System," in *2014 IEEE International Electric Vehicle Conference, IEVC 2014*, 2014, pp. 1–7.

[6] International Association of Public Transport, "Public Transport Trends 2017," Brussels, Belgium, 2017.

[7] A. Lajunen, "Lifecycle costs and charging requirements of electric buses with different charging methods," *J. Clean. Prod.*, vol. 172, pp. 56–67, 2018.

[8] J. R. M. Delos Reyes, R. V. Parsons, and R. Hoemsen, "Winter Happens: The Effect of Ambient Temperature on the Travel Range of Electric Vehicles," *IEEE Trans. Veh. Technol.*, vol. 65, no. 6, pp. 4016–4022, 2016.

[9] Z. Gao *et al.*, "Battery capacity and recharging needs for electric buses in city transit service," *Energy*, vol. 122, pp. 588–600, 2017.

[10] J. Vepsäläinen, K. Kivekäs, K. Otto, and K. Tammi, "Development and Validation of Energy Demand Uncertainty Model for Electric City Buses," *Transp. Res. Part D Transp. Environ.*, vol. 63, pp. 347–361, 2018.

[11] X. He *et al.*, "Energy consumption and well-to-wheels air pollutant emissions of battery electric buses under complex operating conditions and implications on fleet electrification," *J. Clean. Prod.*, vol. 171, pp. 714–722, 2018.

[12] I. S. Suh, M. Lee, J. Kim, S. T. Oh, and J. P. Won, "Design and experimental analysis of an efficient HVAC (heating, ventilation, air-conditioning) system on an electric bus with dynamic on-road wireless charging," *Energy*, vol. 81, pp. 262–273, 2015.

[13] A. Lajunen, Y. Yang, and A. Emadi, "Recent Developments in Thermal Management of Electrified Powertrains," *IEEE Trans. Veh. Technol.*, vol. 67, no. 12, pp. 11486–11499, 2018.

[14] L. Horrein, A. Bouscayrol, W. Lhomme, and C. Depature, "Impact of Heating System on the Range of an Electric Vehicle," *IEEE Trans. Veh. Technol.*, vol. 66, no. 6, pp. 4668–4677, 2017.

[15] A. Lajunen, "Energy Efficiency and Performance of Cabin Thermal Management in Electric Vehicles," *SAE Tech. Pap.*, 2017.

[16] D. Göhlich, T. A. Ly, A. Kunith, and D. Jefferies, "Economic assessment of different air-conditioning and heating systems for electric city buses based on comprehensive energetic simulations," *World Electr. Veh. J.*, vol. 7, no. 3, pp. 398–406, 2015.

[17] Q. Peng and Q. Du, "Progress in heat pump air conditioning systems for electric vehicles-A review," *Energies*, vol. 9, no. 4, 2016.

[18] A. Lajunen, K. Kivekäs, F. Baldi, J. Vepsäläinen, and K. Tammi, "Different approaches to improve energy consumption of battery electric buses," in *2018 IEEE Vehicle Power and Propulsion Conference, VPPC 2018*, 2018.

[19] K. Tammi, T. Minav, and J. Kortelainen, "Thirty Years of Electro-Hybrid Powertrain Simulation," *IEEE Access*, 2018.

[20] Z. Younes, L. Boudet, F. Suard, M. Gerard, and R. Rioux, "Analysis of the main factors influencing the energy consumption of electric vehicles," in *Proceedings of the 2013 IEEE International Electric Machines and Drives Conference, IEMDC 2013*, 2013, pp. 247–253.

[21] C. Fiori, K. Ahn, and H. A. Rakha, "Power-based electric vehicle energy consumption model: Model development and validation," *Appl. Energy*, vol. 168, pp. 257–268, 2016.

[22] A. Kontou and J. Miles, "Electric Buses: Lessons to be Learnt from the Milton Keynes Demonstration Project," *Procedia Eng.*, vol. 118, pp. 1137–1144, 2015.

[23] J. Vepsäläinen, A. Ritari, A. Lajunen, K. Kivekäs, and K. Tammi, "Energy Uncertainty Analysis of Electric Buses," *Energies*, vol. 11, no. 12, p. 3267, 2018.

[24] J. Asamer, A. Graser, B. Heilmann, and M. Ruthmair, "Sensitivity analysis for energy demand estimation of electric vehicles," *Transp. Res. Part D Transp. Environ.*, vol. 46, pp. 182–199, 2016.

[25] A. Lajunen and K. Tammi, "Energy consumption and carbon dioxide emission analysis for electric city buses," in *EVS29 Symposium*, 2016, pp. 1–12.

[26] J. Vepsäläinen, "Driving Style Comparison of City Buses: Electric vs. Diesel," in *2017 IEEE Vehicle Power and Propulsion Conference, VPPC 2017*, 2017.

[27] A. Lajunen, "Energy consumption and cost-benefit analysis of hybrid and electric city buses," *Transp. Res. Part C Emerg. Technol.*, vol. 38, pp. 1–15, 2014.

[28] L. Zeng, T. W. Ching, W. Li, K. T. Chau, and C. C. Chan, "Application of Electric and Hybrid Electric Buses in Macau," in *EVS29 Symposium*, 2016, pp. 1–10.

[29] B. Zhou *et al.*, "Real-world performance of battery electric buses and their life-cycle benefits with respect to energy consumption and carbon dioxide emissions," *Energy*, vol. 96, pp. 603–613, 2016.

[30] K. Kivekäs, A. Lajunen, J. Vepsäläinen, and K. Tammi, "City Bus Powertrain Comparison: Driving Cycle Variation and Passenger Load Sensitivity Analysis," *Energies*, vol. 11, no. 7, 2018.

[31] J. Vepsäläinen, K. Otto, A. Lajunen, and K. Tammi, "Computationally efficient model for energy demand prediction of electric city bus in varying operating conditions," *Energy*, vol. 169, pp. 433–443, 2018.

[32] K. Kivekas, J. Vepsäläinen, and K. Tammi, "Stochastic Driving Cycle Synthesis for Analyzing the Energy Consumption of a Battery Electric Bus," *IEEE Access*, vol. 6, pp. 55586–55598, 2018.

[33] H. Liimatainen, "Utilization of fuel consumption data in an ecodriving incentive system for heavy-duty vehicle drivers," *IEEE Trans. Intell. Transp. Syst.*, vol. 12, no. 4, pp. 1087–1095, 2011.

[34] W. T. Lai, "The effects of eco-driving motivation, knowledge and reward intervention on fuel efficiency," *Transp. Res. Part D Transp. Environ.*, vol. 34, pp. 155–160, 2015.

[35] Q. Cheng, L. Nouveliere, and O. Orfila, "A new eco-driving assistance system for a light vehicle: Energy management and speed optimization," in *IEEE Intelligent Vehicles Symposium, Proceedings*, 2013, no. June, pp. 1434–1439.

[36] F. Mensing, E. Bideaux, R. Trigui, and H. Tattegrain, "Trajectory optimization for eco-driving taking into account traffic constraints," *Transp. Res. Part D Transp. Environ.*, vol. 18, no. 1, pp. 55–61, 2013.

[37] F. Mensing, E. Bideaux, R. Trigui, J. Ribet, and B. Jeanneret, "Eco-driving: An economic or ecologic driving style?," *Transp. Res. Part C Emerg. Technol.*, vol. 38, pp. 110–121, 2014.

[38] A. Lajunen, "Energy-optimal velocity profiles for electric city buses," in *IEEE International Conference on Automation Science and Engineering*, 2013, pp. 886–891.

[39] H. Lim, W. Su, and C. C. Mi, "Distance-Based Ecological Driving Scheme Using a Two-Stage Hierarchy for Long-Term Optimization and Short-Term Adaptation," *IEEE Trans. Veh. Technol.*, vol. 66, no. 3, pp. 1940–1949, 2017.

[40] E. Ozatay *et al.*, "Cloud-based velocity profile optimization for everyday driving: A dynamic-programming-based solution," *IEEE Trans. Intell. Transp. Syst.*, vol. 15, no. 6, pp. 2491–2505, 2014.

[41] V.-D. Doan, H. Fujimoto, S. Member Takafumi Koseki, T. Yasuda, M. Hiroyuki Kishi, and T. Fujita, "Iterative Dynamic Programming for Optimal Control Problem with Isoperimetric Constraint and Its Application to Optimal Eco-driving Control of Electric Vehicle," *IEEJ J. Ind. Appl.*, vol. 7, no. 1, pp. 80–92, 2018.

[42] X. Zeng and J. Wang, "A Parallel Hybrid Electric Vehicle Energy Management Strategy Using Stochastic Model Predictive Control With Road Grade Preview," *IEEE Trans. Control Syst. Technol.*, vol. 23, no. 6, pp. 2416–2423, 2015.

[43] S. Zhang, R. Xiong, and F. Sun, "Model predictive control for power management in a plug-in hybrid electric vehicle with a hybrid energy storage system," *Appl. Energy*, vol. 185, pp. 1654–1662, 2017.

[44] M. Salazar, C. Balerna, P. Elbert, F. P. Grando, and C. H. Onder, "Real-time control algorithms for a hybrid electric race car using a two-level model predictive control scheme," *IEEE Trans. Veh. Technol.*, vol. 66, no. 12, pp. 10911–10922, 2017.

[45] C. Xiang, F. Ding, W. Wang, and W. He, "Energy management of a dual-mode power-split hybrid electric vehicle based on velocity prediction and nonlinear model predictive control," *Appl. Energy*, vol. 189, pp. 640–653, 2017.

[46] S. Xie, X. Hu, Z. Xin, and L. Li, "Time-Efficient Stochastic Model Predictive Energy Management for a Plug-In Hybrid Electric Bus with an Adaptive Reference State-of-Charge Advisory," *IEEE Trans. Veh. Technol.*, vol. 67, no. 7, pp. 5671–5682, 2018.

[47] M. A. S. Kamal, J. I. Imura, T. Hayakawa, A. Ohata, and K. Aihara, "Smart driving of a vehicle using model predictive control for improving traffic flow," *IEEE Trans. Intell. Transp. Syst.*, vol. 15, no. 2, pp. 878–888, 2014.

[48] B. Ren, H. Zhao, W. Deng, and H. Chen, "Model predictive control allocation for stability improvement of four-wheel drive electric vehicles in critical driving condition," *IET Control Theory Appl.*, vol. 9, no. 18, pp. 2688–2696, 2015.

[49] D. Rubin and S. A. Arogeti, "Vehicle yaw stability control using active limited-slip differential via model predictive control methods," *Veh. Syst. Dyn.*, vol. 53, no. 9, pp. 1315–1330, 2015.

[50] M. A. Abbas, R. Milman, and J. M. Eklund, "Obstacle Avoidance in Real Time with Nonlinear Model Predictive Control of Autonomous Vehicles," *Can. J. Electr. Comput. Eng.*, vol. 40, no. 1, pp. 12–22, 2017.

[51] J. Ji, A. Khajepour, W. W. Melek, and Y. Huang, "Path planning and tracking for vehicle collision avoidance based on model predictive control with multiconstraints," *IEEE Trans. Veh. Technol.*, vol. 66, no. 2, pp. 952–964, 2017.

[52] J. Lopez-Sanz *et al.*, "Nonlinear model predictive control for thermal management in plug-in hybrid electric vehicles," *IEEE Trans. Veh. Technol.*, vol. 66, no. 5, pp. 3632–3644, 2017.

[53] R. Wang, G. Xiao, and P. Wang, "Hybrid Centralized-Decentralized (HCD) Charging Control of Electric Vehicles," *IEEE Trans. Veh. Technol.*, vol. 66, no. 8, pp. 6728–6741, 2017.

[54] J. Suh, H. Chae, and K. Yi, "Stochastic Model-Predictive Control for Lane Change Decision of Automated Driving Vehicles," *IEEE Trans. Veh. Technol.*, vol. 67, no. 6, pp. 4771–4782, 2018.

[55] S. Wei, Y. Zou, X. Zhang, T. Zhang, and X. Li, "An Integrated Longitudinal and Lateral Vehicle Following Control System with Radar and Vehicle-to-Vehicle Communication," *IEEE Trans. Veh. Technol.*, vol. 68, no. 2, pp. 1116–1127, 2019.

[56] M. A. S. Kamal, M. Mukai, J. Murata, and T. Kawabe, "On board eco-driving system for varying road-traffic environments using model predictive control," in *Proceedings of the IEEE International Conference on Control Applications*, 2010, no. October, pp. 1636–1641.
[57] M. Vajedi and N. L. Azad, "Ecological adaptive cruise controller for plug-in hybrid electric vehicles using nonlinear model predictive control," *IEEE Trans. Intell. Transp. Syst.*, vol. 17, no. 1, pp. 113–122, 2016.
[58] M. Held, O. Flärdh, and J. Mårtensson, "Optimal Speed Control of a Heavy-Duty Vehicle in Urban Driving," *IEEE Trans. Intell. Transp. Syst.*, pp. 1–12, 2018.
[59] S. Zhang, Y. Luo, K. Li, and V. Li, "Real-Time Energy-Efficient Control for Fully Electric Vehicles Based on an Explicit Model Predictive Control Method," *IEEE Trans. Veh. Technol.*, vol. 67, no. 6, pp. 4693–4701, 2018.
[60] "Nonlinear MPC Controller," *MathWorks*, 2018. [Online]. Available: https://se.mathworks.com/help/mpc/ref/nonlinearmpccontroller.html. [Accessed: 30-Dec-2018].
[61] T. Sourander, "Kaupunkibussien kevytrakennetekniikka," Aalto University, 2013.
[62] Linkker, "Technology," 2018. [Online]. Available: http://www.linkkerbus.com/technology/. [Accessed: 14-Feb-2018].
[63] Volvo Bus Corporation, "Volvo 7900 Electric Specifikationer," 2018. [Online]. Available: http://www.volvobuses.se/sv-se/our-offering/buses/volvo-7900-electric/specifications.html. [Accessed: 08-May-2018].
[64] W.-H. Hucho *et al.*, *Aerodynamics of Road Vehicles: From Fluid Mechanics to Vehicle Engineering*, 1st ed. Cambridge, UK: Elsevier, 1987.
[65] "Rolling Resistance and Rolling Noise Limits for Truck and Bus Tires according to UN Regulation 117," *Continental Tires*, 2018. [Online]. Available: https://www.continental-tires.com/transport/knowhow/un-regulation-117. [Accessed: 30-Dec-2018].
[66] T. Halmeaho *et al.*, "Experimental validation of electric bus powertrain model under city driving cycles," *IET Electr. Syst. Transp.*, vol. 7, no. 1, pp. 74–83, 2016.
[67] M. Morari and J. Lee, "Model Predictive Control: Past, Present and Future," *Comput. Chem. Eng.*, vol. 23, no. 4–5, pp. 667–682, 1999.

KLAUS KIVEKÄS (S'18) was born in Espoo, Finland in 1991. He received BSc and MSc degrees in mechanical engineering from Aalto University in 2015 and 2016.

In 2013, he worked as a Research Assistant at the Fluid Power laboratory at Aalto University. Since 2016, Klaus has been a Doctoral Candidate in the Department of Mechanical Engineering at Aalto University. His research interests include alternative city bus powertrain topologies and city bus energy consumption uncertainty.

ANTTI LAJUNEN (M'10–SM'18) received the M.Sc. degree in Mechanical Engineering from Helsinki University of Technology, Espoo, Finland, in 2005 and Master of Advanced Studies degree in Industrial Engineering from Ecole Centrale Paris (ECP), Paris, France, in 2007. He received his D.Sc. in 2014 from Aalto University, Espoo, Finland.

He is currently working as an Assistant Professor in Agricultural Engineering at the University of Helsinki, Finland. His main research interests are vehicle electrification, modeling and simulation of agricultural vehicles and machinery, and automation in agriculture.

FRANCESCO BALDI (M'15) earned his BSc and MSc degrees in Energy Engineering at the University of Bologna, in Italy. In 2016 he successfully defended his PhD thesis on Modelling, Analysis and Optimization of Ship Energy Systems at Chalmers University of Technology in Sweden.

After that, Francesco worked for two years on the ODes aCCSES project on the Optimal Design and Control of Cruise Ship Energy Systems, between EPFL (CH) and Aalto University (FI). Since 2019 Francesco works as a researcher in the ENEA research center (IT), working on the improvement of energy efficiency in the industrial and public sectors.

JARI VEPSÄLÄINEN (S'17) received B.Sc. and M.Sc. degrees at Aalto University in 2014 and 2016.

During his studies, he concurrently worked as a Research Assistant in the Fluid Power laboratory. Jari is currently continuing his academic career as a Doctoral Candidate at Aalto University, a position he has held since 2016. During his doctoral studies, he has also been involved in course planning and assisting in teaching of mechatronics.

KARI TAMMI (M'13) received MSc, LicSc, and DSc degrees at Helsinki University of Technology in 1999, 2003, and 2007. He received a Teacher's pedagogical qualification at Häme University of Applied Sciences in 2017.

He has worked as an Associate Professor at Aalto University since 2015. Kari also serves the Finnish Administrative Supreme Court as Chief Engineer Counselor. Earlier, he worked as Research Professor, Research Manager, Team Leader and other positions at VTT Technical Research Centre of Finland (2000-2015). He was a post-doctoral researcher at North Carolina State University (USA, 2007-2008), and a researcher at CERN, the European Organization for Nuclear Research in 1997-2000. He has authored more than 60 peer-reviewed publications cited in more than 1500 other publications. Dr. Tammi serves as the deputy chair for IFTOMM Finland, and he is a member of the Finnish Academy of Technology.